Interactions between Lattice Dislocations and Grain Boundaries in Ni3Al Investigated by Means of In Situ TEM and Computer Modelling Experiments

Pestman, B.J.; De Hosson, J.T.M.

Published in:
Acta Metallurgica et Materialia

DOI:
10.1016/0956-7151(92)90321-5

Publication date:
1992

Acta metall. mater. Vol. 40, No. 10, pp. 2511–2521, 1992
Printed in Great Britain.

0956-7151/92 $5.00 + 0.00

INTERACTIONS BETWEEN LATTICE DISLOCATIONS AND GRAIN BOUNDARIES IN Ni_3Al INVESTIGATED BY MEANS OF *IN SITU* TEM AND COMPUTER MODELLING EXPERIMENTS

B. J. PESTMAN and J. Th. M. DE HOSSON

Department of Applied Physics, Materials Science Center, University of Groningen, Nijenborgh 18, 9747 AG Groningen, The Netherlands

(Received 25 November 1991; in revised form 25 March 1992)

Abstract—The interaction between lattice dislocations and grain boundaries in Ni_3Al has been investigated by means of *in situ* TEM deformation experiments. The interaction between screw dislocations and a coherent twin boundary could be analyzed in detail. The interaction mechanism found experimentally was compared to the results of a computer modelling study. In the computer modelling study, many-body potentials representing Ni_3Al were used. The results of the *in situ* straining indicate that $\langle 110 \rangle$ screw dislocations impinging on a $\Sigma = 3$ coherent twin boundary that have a Burgers vector that is parallel to the grain boundary plane can be transmitted to the symmetric slip plane in the other grain under influence of an applied stress. A one-to-one comparison with the results of a computer modelling study of exactly the same system in Ni_3Al can be made and the experiment agrees with the simulations. Also, observations were made of superlattice intrinsic stacking faults (SISF) that were formed as a result of the interaction between gliding dislocations and the dislocations of a low angle grain boundary (cell wall). The creation of jogs in the line of the gliding dislocation may be the cause of the SISF formation.

Résumé—On étudie l'interaction entre les dislocations du réseau et les joints de grains dans Ni_3Al au moyen d'essais de déformation *in situ* en MET. L'interaction entre les dislocations vis et un joint de macle cohérent peut être analysée en détail. Le mécanisme d'interaction trouvé expérimentalement est comparé aux résultats d'une étude modélisée par ordinateur. Dans l'étude modélisée, on utilise des potentiels à n corps pour représenter Ni_3Al. Les résultats des déformations *in situ* montrent que les dislocations vis $\langle 110 \rangle$ qui rencontrent un joint de macle cohérent $\Sigma = 3$, ayant un vecteur de Burgers parallèle au plan du joint de grains, peuvent être transmises sur le plan de glissement symétrique de l'autre grain sous l'action de la contrainte appliquée. Une comparaison point par point avec les résultats de l'étude numérique du même système dans Ni_3Al peut être effectuée et l'expérience est en accord avec les simulations. De plus, on observe des défauts d'empilement intrinséques de surstructure qui se sont formés par suite de l'interaction entre les dislocations qui glissent et celles d'un joint de grains de faible désorientation (paroi de cellule). La création de crans sur la ligne de la dislocation qui glisse peut être la cause de la formation d'un tel défaut.

Zusammenfassung—Die Wechselwirkung zwischen Gitterversetzungen und Korngrenzen in Ni_3Al wird mit *in-situ*-Verformungsexperimenten im Durchstrahlungselektronenmikroskop untersucht. Die Wechselwirkung zwischen Schraubenversetzungen und einer kohärenten Zwillingsgrenze kann ausführlich analysiert werden. Der gefundene Wechselwirkungsmechanismus wird mit den Ergebnissen einer Computer-Modellstudie verglichen. In dieser werden Vielkörperpotentiale, die das Ni_3Al darstellen, benutzt. Aus den Ergebnissen geht hervor, daß eine auf die kohärente Zwillingsgrenze $\Sigma = 3$ auftreffende $\langle 110 \rangle$-Schraubenversetzungen unter dem Einfluß einer äußeren Spannung auf die symmetrische Gleitebene im Nachbarkorn gebracht werden kann, wenn ihr Burgersvektor in der Zwillingsgrenzenebene liegt. Dieser Fall kann mit den Computerexperiment an genau demselben System im Ni_3Al eins-zu-eins verglichen werden; die Simulation stimmt mit dem Experiment überein. Außerden werden intrinsische Stapelfehler des Übergitters, die sich durch die Wechselwirkung von Gleitversetzungen mit den Versetzungen einer Kleinwinkelkorngrenze (Zellwand) ergeben, beobachtet. Die Ursache dieser Stapelfehler kann darin leigen, daß sich Versetzungssprünge in den Gleitversetzungen bilden.

INTRODUCTION

Ni_3Al, which has an $L1_2$ structure, is an ordered compound that is a very promising candidate for various high temperature applications, such as turbine blades for the aircraft industry. Its application has been hampered because Ni_3Al in its polycrystalline form exhibits brittle fracture along the grain boundaries. Aoki and Izumi [1] showed that the ductility at room temperature of Ni-rich polycrystalline Ni_3Al can be improved notably by addition of small amounts of boron. However, the increase in ductility drops again at high temperatures. If useful structural materials based on these intermetallic

ordered compounds are ever to be further developed, it is crucial to scrutinize the reasons for their brittle behaviour. A possible reason could be found in low cohesion of the grain boundaries.

However, there exists experimental evidence that in Ni_3Al the dislocation mobility in the vicinity of grain boundaries may be strongly enhanced when ductilization takes place [2] and that plastic flow precedes inter-granular fracture [3]. Considering these experiments, it might be reasoned that the passage of gliding dislocations arriving from the lattice might be hindered by grain boundaries. The results of computer modelling studies [4–5] indicate that grain boundaries in $L1_2$ ordered compounds hinder dislocation motion. This effect increases with higher ordering tendency.

Various approaches exist to the experimental study of the interaction between lattice dislocations and grain boundaries, such as slip line analysis [6] and etch-pitting [7]. However, these techniques are not capable of giving information about the nature of the dislocation and the grain boundary, such as the line direction and the Burgers vector of a dislocation, the orientation of the grain boundary plane and the misorientation between the two grains. Transmission electron microscopy is a technique that allows observation of defect configurations in thin foils and also provides information of the nature of the defects. In many experiments [8, 9], bulk samples of different materials have been deformed and these samples have been prepared for study in the TEM. Although a full analysis of the dislocation–grain boundary configuration is possible, the development of the interaction has to be deduced from the configuration that is left behind after the interaction has taken place.

In situ deformation in a TEM is one of the very few techniques by which the development of the interaction between lattice dislocations and grain boundaries can be studied and which at the same time allows to analyze the configuration. By this technique, samples which have not yet been deformed, are strained inside a TEM in a special straining holder. In practice there are a number of complexities. It is always possible that there is a substantial influence of the fact that the interaction is studied in a very thin foil, while we are interested in bulk properties: the electron transparent region may have a complicated geometry because of the thinning and therefore the stresses in the thin region may be different from the bulk stress state. Further, an oxide layer on the surfaces may hinder the motion of dislocations. Nevertheless, in many cases the *in situ* TEM technique is a promising tool for investigations of dislocation–grain boundary interactions.

EXPERIMENTS

In situ deformation

Ni_3Al was prepared by arc-melting 99.99% pure Ni and 99.999% pure Al. The material was homogenized at 1100°C (1373 K) for 5 days, resulting in grain sizes of 1 mm. Miniature tensile specimens (6 × 3 mm, with a thickness of 350 μm) were cut out of the bulk material by spark erosion. There were two holes in the sample through which it was held by the pins of the two grips of the deformation holder. The sample was necked in the middle, so as to maximize the likelihood that the deformation would start near the future electron transparent region. Care was taken to have a grain boundary, preferably a coherent twin boundary, present in the middle of the sample.

Next, the sample had to be thinned, to obtain an electron transparent region. First, the sample was ground to a thickness of 150 μm using a Gatan disc grinder and then the sample was dimpled on both sides of the location of the grain boundary, reducing the thickness locally from 150 μm to around 60 μm. This was done to increase the probability of having the grain boundary in the thin area. The last step of the preparation process was the final thinning of the specimen in a Struers Tenupol electropolishing unit, using a mixture of 70% methanol and 30% nitric acid at 0°C, at an applied voltage of 8 V.

For observation of the specimen, a JEM 200-CX was used, which was operated at 200 kV. The specimen was mounted in a special single tilt *in situ* deformation holder, built on principles taken from Kubin and Veyssière [10] (Fig. 1). In the deformation holder, the sample is strained by means of a vacuum system, which is operated from outside the microscope. In this way the sample is deformed at constant load. The processes during deformation could be monitored by a TV-system and could be recorded on video. The deformation was stopped before total disruption of the specimen. After the *in situ* deformation, specimens that promised to be interesting were shaped into 3 mm diameter discs by very cautious grinding, taking care that the thin area was protected. In this way they fitted in a double tilt holder and the defects could be analyzed in detail.

Computer modelling experiments

In the modelling study, Finnis–Sinclair potentials representing Ni_3Al [11] were used for the description of interatomic forces. For the simulations, the following procedure was used. First, the grain boundary was relaxed, using a standard gradient method; details are described elsewhere [12]. Secondly, a computational block for the relaxation of the dislocation near the grain boundary was constructed. The computational block of the relaxed grain boundary was extended, according to the periodicity of the CSL, to form a block of more than $40\,b \times 40\,b$ (b is the magnitude of the Burgers vector) perpendicular to the dislocation line. Next, the displacement field of a $\frac{1}{2}[110]$ dislocation was imposed with its elastic center initially positioned at such a distance from the grain boundary that there was no strong effect of the grain boundary on the relaxation of the dislocation core.

Fig. 1. The *in situ* deformation holder with a sample mounted. 1: fixed grip, 2: sample, 3: thermocouple (not used), 4: moveable grip.

Along the dislocation line, periodic boundary conditions were applied. The anisotropic elastic solution (as if there was only one grain present) was used for the boundary conditions perpendicular to the dislocation line. The displacement field of $\frac{1}{2}[110]$ superpartial was imposed with its elastic centre near the boundary plane, connected by a ribbon of anti phase boundary (APB) to another superpartial at elastic equilibrium distance, according to the APB energy. The initial position of the core was always chosen such that dissociation would occur on the glide plane [13, 14]. The dislocation–grain boundary relaxation was carried out in the usual way for dislocation relaxation [15].

After relaxation of the dislocation core, a homogeneous shear strain was imposed on the computational block, corresponding to a shear stress, as prescribed by anisotropic elasticity theory (as if only the grain initially containing the dislocation was present). The shear stress was applied in the direction of the Burgers vector, such that the dislocation would move towards the grain boundary plane. The simulations started with imposing a shear strain corresponding to a small stress. Larger stresses were built up by repeating this process.

RESULTS

In situ deformation

In many samples, cracks (some of which were already present before the deformation started) were observed that had initiated at the edge of the thin foil, propagating along {111} planes. Dislocations were often seen to be emitted from the crack tip, in the plane of the crack and sometimes also on inclined planes. In addition, observations were made of dislocations arriving from the bulk, although these observations were not so numerous. The dislocations from the bulk never arrived all on the same slip plane, but seemed to appear in slip bands. Quite frequently, the propagation of the crack occurred in a jerky type of motion and then, it was impossible to observe any dislocation motion.

In many of the specimens there was a grain boundary, often a coherent twin boundary ($\Sigma = 3$, 109.47° around [110] with boundary plane $(\bar{1}11)$), visible in the electron transparent region. A number of observations were made of individual dislocations that had been emitted from cracks. Sometimes dislocations arriving from the bulk impinged on twin boundaries and were arrested at the boundary plane. Cracks were seen that had grown through a twin boundary and had changed their direction of propagation upon crossing of the boundary plane.

Interaction with a $\Sigma = 3$ coherent twin boundary

One sample showed a crack which had grown during the *in situ* deformation to the close vicinity of a coherent twin boundary, but which had not crossed the boundary.

On the other side of the boundary, starting exactly from the line of intersection of the crack plane and the boundary plane, slip traces could be observed leading into the other grain, to a large number of dislocations that all had the same slip plane (Fig. 2).

This sample was chosen for further analysis in the double tilt holder. The rotation of the boundary under study could be described within the error margins as a 109.5° rotation around [110], characteristic for a twin boundary. By tilting to an edge-on position, the boundary plane was determined to be $(\bar{1}11)$, which is equal to $(\bar{1}1\bar{1})_{II}$. The index II indicates the coordinate system of the grain containing the dislocations. The grain containing the crack is meant if no index is used. In a similar way, the plane of the crack was determined to be close to $(1\bar{1}1)$ and the slip plane of the dislocations was determined to be $(1\bar{1}\bar{1})_{II}$. By the $\mathbf{g}\cdot\mathbf{b} = 0$ invisibility criterion, the Burgers vector of the dislocations was determined to be parallel to $[110]_{II}$; this is the [110] direction that is common to both grains. The line direction was

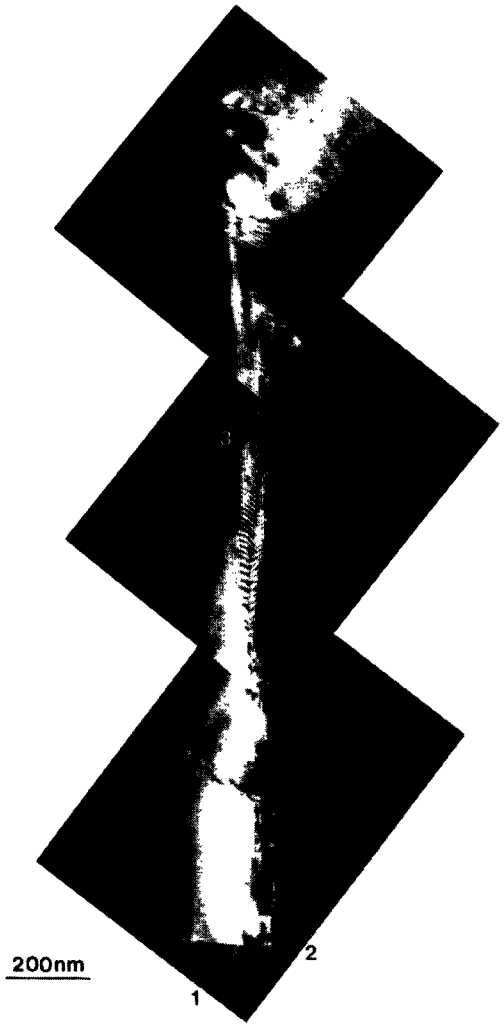

Fig. 2. The dislocation configuration that was found attached to the slip lines. 1: crack, 2: boundary plane, 3: dislocation array.

determined to be $[230]_{II} \pm 13°$, which is close to the $[110]_{II}$ screw direction.

Interaction with low-angle grain boundaries

In one sample, in the thin electron transparent region many low-angle grain boundaries were present, but no high angle grain boundaries were visible. In this sample there were only a few holes of approximately 5 μm in diameter and there were no cracks in the sample at all, contrary to most samples that contained a hole of about 50 μm in diameter and a few small initial cracks. The external force that had to be applied to cause deformation in the thin region was twice as high as usual for samples of the same thickness. This might be explained by the absence of stress concentrations because of cracks or large holes. During the experiment, many dislocations were seen gliding, almost exclusively in one slip band, in parallel planes. It was observed that at several places elongated stacking faults, hundreds of nanometers long, had been created at the intersections of the slip

Fig. 3. Stacking fault near a low-angle grain boundary (arrows), showing characteristic fringe contrast.

band with low-angle grain boundaries, see Fig. 3. The faults always lay at the same side of the boundaries: the direction of motion of the gliding dislocations always pointed from the boundary to the faults. Thus, it can be assumed that the faults have been created by interaction of the gliding dislocations with the dislocations in the boundary. Also at several other locations along the slip band, away from the intersections with low angle grain boundaries, gliding dislocations had formed faults. The deformation experiment was stopped after a crack had developed, originating from one of the holes. The sample was shaped into a 3 mm disc for further investigation in a double tilt holder. One of the intersections of the slip band with a low-angle grain boundary where faults had formed was chosen for detailed analysis. Three faults can be seen that are close to three dislocations in the low-angle grain boundary, at distances varying from less than 50–200 nm, see Fig. 4.

The foil normal was $[10\,3\,11] \pm 3°$, which is 11° from [101] and the foil thickness at the point of interest was 110 ± 15 nm. If we assume that the

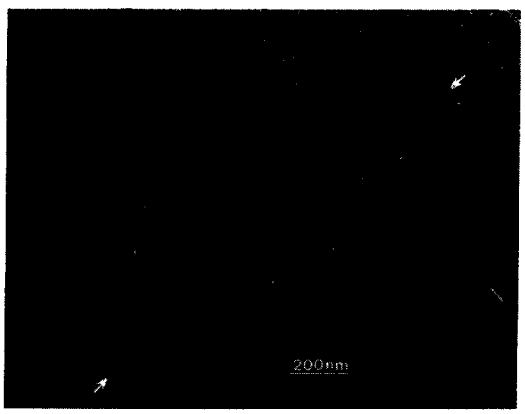

Fig. 4. Weak-beam micrograph of superlattice intrinsic stacking faults (SISFs) near a low-angle grain boundary. The arrows indicate the location of the low angle grain boundary or cell wall, consisting of an array of parallel dislocations spaced about 200 nm. Only one of the three SISFs can be seen fully; the other two are only partially in view.

Table 1. Values of sin α for different reflections (g's) and fault vectors $\mathbf{R}_f$

$\mathbf{R}_f$	$\mathbf{g}=[002]$	$\mathbf{g}=[00\bar{2}]$
$+1/3\ [1\bar{1}1]$	$-1/2\sqrt{3}$	$1/2\sqrt{3}$
$-1/3\ [1\bar{1}1]$	$1/2\sqrt{3}$	$-1/2\sqrt{3}$

macroscopic tensile axis was perpendicular to the foil normal and parallel to the line connecting the two grips by which the sample was held, this axis could be determined to be $[4\bar{7}\bar{2}] \pm 10°$. It has to be noted that similar fault configurations close to a low-angle grain boundary have also been observed in thicker parts of the specimen, further down the same slip band. The average line direction of the dislocations constituting the low-angle grain boundary was $[02\bar{5}] \pm 5°$. The dislocations in the boundary had two different Burgers vectors: $[1\bar{1}0]$ or [110]. The dislocations that were close to the faults all had a Burgers vector $[1\bar{1}0]$. The dislocations in the boundary that had $\mathbf{b}=[110]$ were dissociated so widely into $\frac{1}{2}$[110]superpartial dislocations in the (100) plane, that the individual partials could be resolved in weak-beam (Fig. 4).

The plane of the faults was determined to be $(1\bar{1}1)$ by tilting the faults to an edge-on position. The fault vector $\mathbf{R}_f$ was determined to be $\pm\frac{1}{3}[1\bar{1}1]$ by applying the invisibility criterion $\alpha = 2\pi\mathbf{g}\cdot\mathbf{R}_f = n\cdot 2\pi$. However, for a fault of this type the positive and the negative fault vector are not equivalent. In one case, a $(1\bar{1}1)$ plane is removed (superlattice intrinsic stacking fault, SISF; this is a shear fault) and in the other case an extra $(1\bar{1}1)$ plane is added (superlattice extrinsic stacking fault, SESF; this is not a shear fault). The exact nature of the fault can be determined in the following way. The contrast of the edge fringe (the fringe at the intersection with the foil surface) in bright field images with $s=0$ depends on the sign of sin α [16]. If sin $\alpha > 0$ the fringe is bright and if sin $\alpha < 0$ the fringe is dark. The values of sin α are listed in Table 1 for reflections which have been used to image the faults in bright field.

The experimental observations were that the edge fringe was dark for $\mathbf{g}=[002]$ and bright for $\mathbf{g}=[00\bar{2}]$, and therefore the fault vector $\mathbf{R}_f$ is $+\frac{1}{3}[1\bar{1}1]$. As the foil normal (pointing upwards) is close to [101], $\mathbf{R}_f$, points to the upper surface of the foil. Thus the fault corresponds to a removal of one $(1\bar{1}1)$ plane and the fault is of intrinsic nature, a SISF.

From the direction of the slip traces left behind by the gliding dislocations it was deduced that the $(1\bar{1}1)$ plane of the faults is the same plane as the slip plane of the gliding dislocations. The faults are partially bounded by the intersection of their $(1\bar{1}1)$ plane and the upper surface of the foil and partially by dislocations with Burgers vector $\pm\frac{1}{3}[\bar{1}12]$ (Fig. 5).

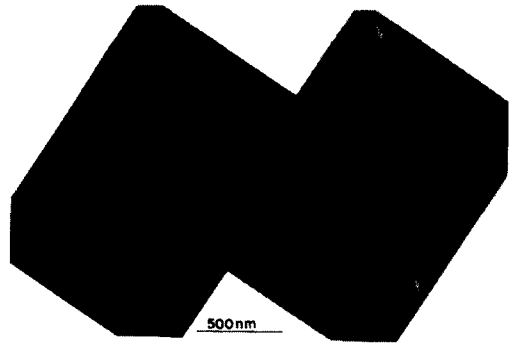

Fig. 5. Weak-beam micrograph of the dislocation partially bounding the faults of Fig. 4. Where not bounded by a dislocation, the faults are bounded by the surface of the thin foil. The fringe contrast of the faults is invisible for this imaging condition. The arrows indicate the location of the low angle grain boundary (cell wall).

The Burgers vector of the dislocations bounding the SISFs has been determined using the $\mathbf{g}\cdot\mathbf{b}$ invisibility criterion. The invisibility criterion for partial dislocations, such as a dislocation bounding a fault, is slightly different from that for perfect dislocations. For a Burgers vector of the type $\frac{1}{3}\langle 112\rangle$, the criterions for invisibility is $\mathbf{g}\cdot\mathbf{b}=0$, $\pm\frac{1}{3}$ [16] and furthermore (for $s>0$) $\mathbf{g}\cdot\mathbf{b}=-\frac{2}{3}$ [17]. Care was taken to use only reflections for which the fault is invisible, to prevent any uncertainty regarding visibility of the dislocation. The dislocations were invisible for $\mathbf{g}=[220]$ and for $\mathbf{g}=[13\bar{1}]$; they were visible for $\mathbf{g}=[022]$, $\mathbf{g}=[1\bar{3}\bar{1}]$ and $\mathbf{g}=[\bar{1}\bar{1}3]$. The $\mathbf{g}\cdot\mathbf{b}$ product for dislocations that can bound an SISF on $(1\bar{1}1)$ is given in Table 2.

From Table 2, it can be concluded that the Burgers vectors of the partial dislocations bounding the SISFs are $\pm\frac{1}{3}[\bar{1}12]$.

Computer modelling

Only the interaction of a $\frac{1}{2}$[110] dislocation of pure screw character with the $\Sigma=3$ $(\bar{1}11)$ ($\Theta = 109.47°$ around [110]) coherent twin boundary was simulated. In this set-up, transmission of the dislocation throughthe grain boundary is relatively easy, as no residue is left behind in the grain boundary plane. In the following, all Miller indices are in the coordinate system of the upper grain, unless otherwise indicated. In the kinematical simulations, the shear stress was applied onto the $(1\bar{1}1)$ plane.

It has to be emphasized that the symbols indicating the atom positions are drawn as if there is no dislocation present. The results for the kinematical

Table 2. $\mathbf{g}\cdot\mathbf{b}$ product for partial dislocations bounding an SISF on $(1\bar{1}1)$

$\mathbf{b}$	$\mathbf{g}=[220]$	$\mathbf{g}=[13\bar{1}]$	$\mathbf{g}=[022]$	$\mathbf{g}=[1\bar{3}\bar{1}]$	$\mathbf{g}=[\bar{1}\bar{1}3]$
$\pm 1/3\ [121]$	2	2	2	−2	0
$\pm 1/3\ [21\bar{1}]$	2	2	0	0	−2
$\pm 1/3\ [\bar{1}12]$	0	0	2	−2	2
$\pm 1/3\ [1\bar{1}1]$	0	−1	0	1	1

simulations are depicted using the differential displacement method [18]. This method indicates the relative displacement of each atom with respect to its neighbours in a certain crystallographic direction (usually the direction of the Burgers vector). If the absolute value of the relative displacement exceeds half of the periodicity of the lattice in that direction (here, $\frac{1}{2}[110]$ was used), an integer number times the period is added or subtracted. The position of the APB is indicated by a line. The relative displacements are indicated by arrows drawn between the atoms.

The $\Sigma = 3$ boundary acted as an obstacle to dislocation motion. The leading $\frac{1}{2}[110]$ superpartial

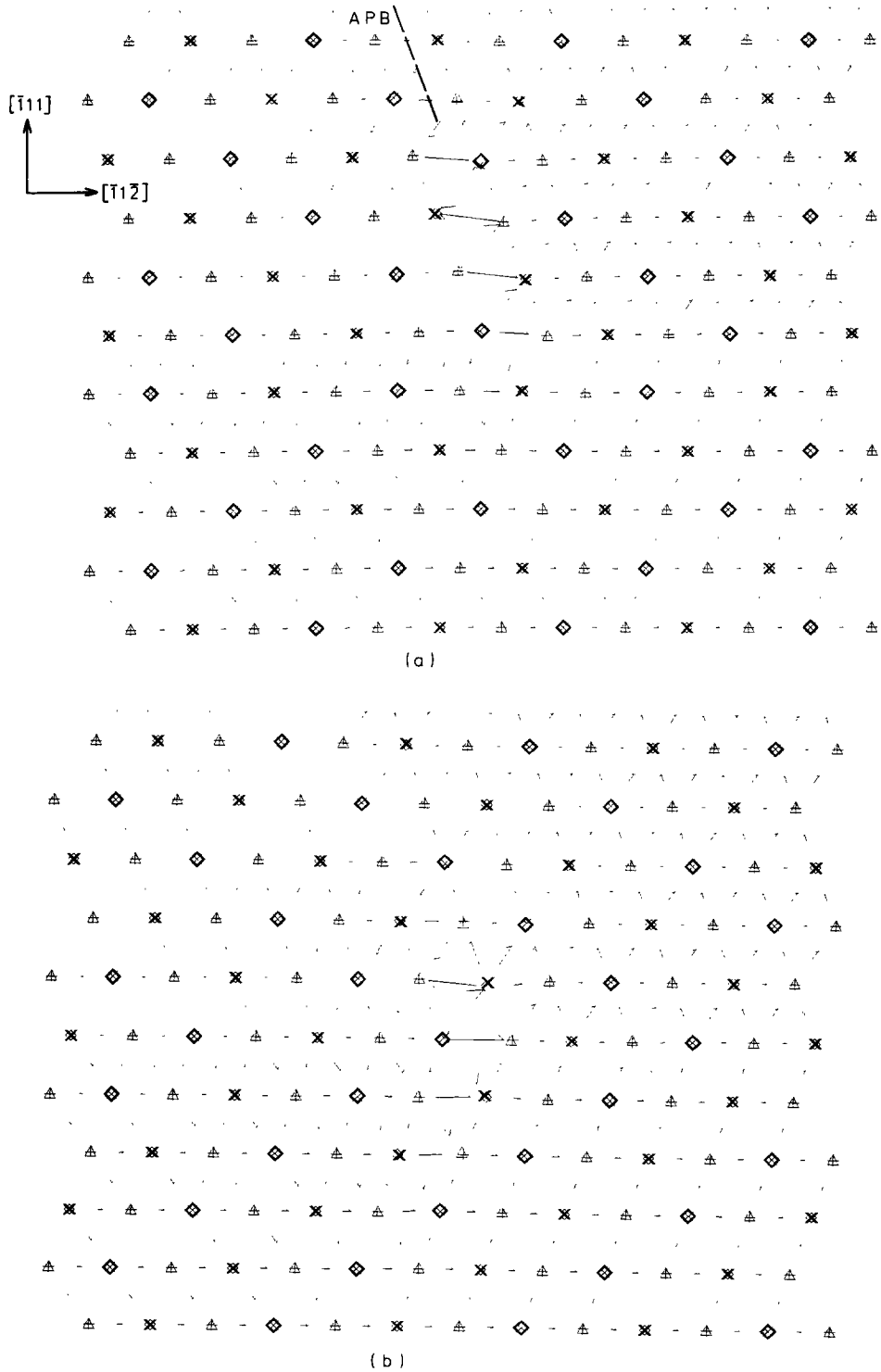

Fig. 6(a, b). *Caption on opposite page.*

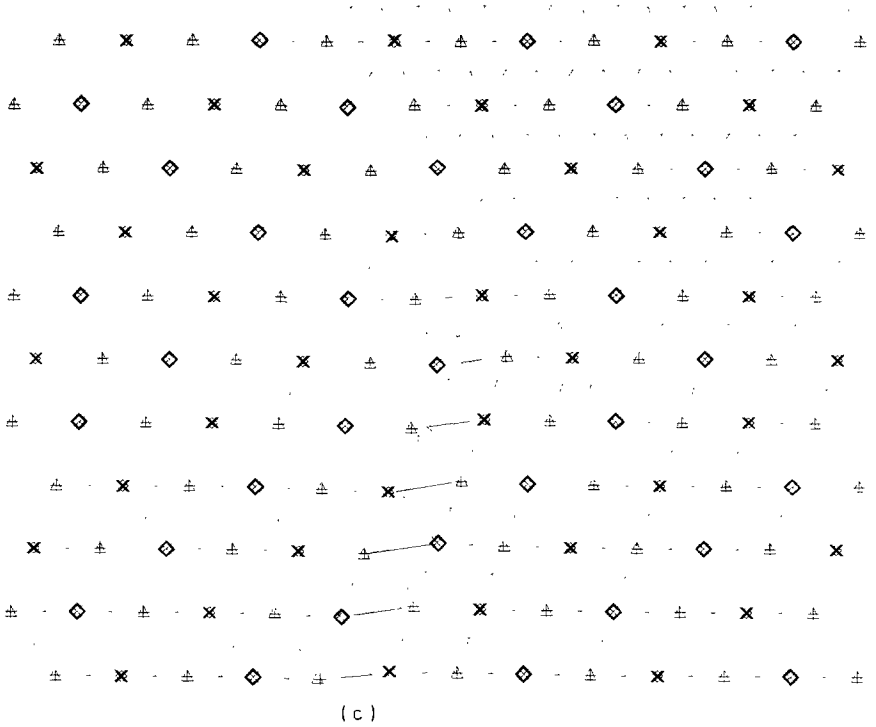

Fig. 6. (a–c) Three stages of the transmission through the $\Sigma = 3$ boundary in Ni_3Al. In these figures, a projection along [110] is shown. The different symbols indicate different heights. Following order: ◇, +, ×, △. The Al atoms are indicated by thicker lines. The position of the APB is indicated by a dashed line. The heights indicated by the symbols are heights before the dislocation was imposed.

dislocation was dissociated into two Shockley partials with very small separation. Upon arrival at the boundary plane, the leading Shockley partial was delayed and a slight decrease of the separation of the Shockleys could be observed. The trailing $\frac{1}{2}[110]$ superpartial dislocation also approached the leading one. When the shear stress reached a level of 4 times the friction stress (the stress, needed to start motion of the dislocation in perfect lattice), transmission occurred across the boundary into the symmetric slip plane $(1\bar{1}\bar{1})_{II}$ in the other grain, see Fig. 6.

DISCUSSION

Interaction with a $\Sigma = 3$ coherent twin boundary

The results of the TEM work show that cracks may emit dislocations parallel to their own plane during propagation. In the case of the sample containing a twin boundary that was analyzed in detail, the plane of the crack crossed a coherent twin boundary ahead of the crack and it might be evisaged that a number of dislocations was emitted from the crack tip in the $(1\bar{1}1)$ plane and impinged on the boundary. The slip traces emanating on the other side of the boundary indicate that a number of dislocations has emerged from the boundary in the $(1\bar{1}\bar{1})_{II}$ plane exactly at the point where the plane of the crack intersects with the boundary plane. Thus, it is probable that these dislocations have been emitted from the crack tip and have been transmitted through the grain boundary. As the [110] direction is common to both grains, the Burgers vector could remain the same in both grains and no residue is left in the boundary. The line vector is parallel to the intersection of crack plane and outgoing slip plane and thus, transmission could occur without rotation of the dislocation line in the boundary plane. The large number of dislocations may indicate that there was a large force on the leading dislocation of a pile-up in front of the boundary, necessary to cause transmission of the dislocations to the other grain. Grain boundary sources of course cannot be ruled out completely as origin of the observed dislocations. However, very often, if operation of grain boundary sources is observed, there is generation of dislocations on many different slip planes [19] (our own observations in two other samples indicate the same), while here, all the dislocations are on one slip plane.

Interaction with low-angle grain boundaries

As low-angle grain boundaries consist of a dislocation network, the interaction between gliding lattice dislocations and low-angle grain boundaries is essentially a dislocation–dislocation interaction. In order to find an explanation for the formation of the SISFs, it is useful to know the type of the dislocations that were gliding in the slip band. Therefore, a number of dislocations that showed such a configuration that it could be expected that they had been gliding in the slip band was analyzed. Most of

the dislocations that were found in the slip band were screw dislocations with Burgers vector [011]. We may assume that the gliding dislocations in the slip band had Burgers vector [011]. This assumption can be supported as follows. If we suppose that the $\frac{1}{3}[\bar{1}12]$ dislocations bounding the SISFs were created by the gliding dislocations, the Burgers vector of the gliding dislocations could either be [011] or $[\bar{1}01]$, as only these dislocations are glissile in the $(1\bar{1}1)$ plane and at the same time can have $\frac{1}{3}[\bar{1}12]$ as one of their dissociation products. If we consider the tensile axis in the thin region to be the same as the macroscopic tensile axis, the Schmid factor for the [011] dislocations in the $(1\bar{1}1)$ plane is 0.38, while the Schmid factor for the $[\bar{1}01]$ dislocations is 0.15. Therefore we conclude that the gliding dislocations had Burgers vector [011]. As the dislocations in the slip band that were analyzed had mostly screw character, we may assume that the gliding dislocations also had screw character. Also it can be expected that the gliding dislocations were dissociated into two $\frac{1}{2}[011]$ superpartials, which is the dissociation that is usually found in Ni_3Al. See Fig. 7 for a schematic overview of the configuration.

Now, we consider the formation mechanism of the SISFs in more detail, see Fig. 8. A gliding dislocation intersects a dislocation in the cell wall. Although the dissociation of the perfect dislocation in the cell wall into superpartial dislocations is not clearly visible, we may assume that it is dissociated in the cell wall into two $\frac{1}{2}[1\bar{1}0]$s. Because of the intersection, 2 jogs have been created in the line of the gliding dislocation, which act as pinning points. As the separation between the two $\frac{1}{2}[1\bar{1}0]$s in the cell wall is very small, the jogs are very close to each other. The [011] dislocation will bow out at both sides of the pinning point under the influence of the stress [Fig. 8(b)]. The leading $\frac{1}{2}[011]$ superpartial dislocation can be allowed to move under the applied stress in the following way: if a $\frac{1}{6}[21\bar{1}]$ Shockley partial dislocation moves from the trailing to the leading superpartial, the APB separating the $\frac{1}{2}[011]$ partials is transformed into SISF, which has much lower energy. By the exchange, the trailing $\frac{1}{2}[011]$ superpartial transforms to a $\frac{1}{3}[\bar{1}12]$ dislocation partially bounding the SISF [Fig. 8(c)].

In this way, the force keeping the two $\frac{1}{2}[011]$ dislocations together because of the high APB energy is greatly reduced as the SISF energy is much lower than the APB energy and thus, the leading $\frac{1}{2}[011]$, together with the $\frac{1}{6}[21\bar{1}]$ can proceed and then a large region of SISF can be formed [Fig. 8(d)]. It might be envisaged that the termination of the SISF region develops in a similar way as the loop pinching mechanism described by Pak *et al.* [20]. See the text below for a brief description. In our case, we are dealing with a partial loop that is bounded by the foil surface and no next loop of SISF is created, but instead a new [011] perfect dislocation might be formed, which proceeds in the $(1\bar{1}1)$ plane.

There have been a number of other observations of SISFs in ordered alloys like Ni_3Al. Baker and Schulson [21] observed in Ni_3Al pairs of $\frac{1}{3}\langle 112\rangle$ dislocations with SISF between, separated around 100 nm. The $\frac{1}{3}\langle 112\rangle$ pairs had parallel Burgers vector and antiparallel line vector. These pairs were thought

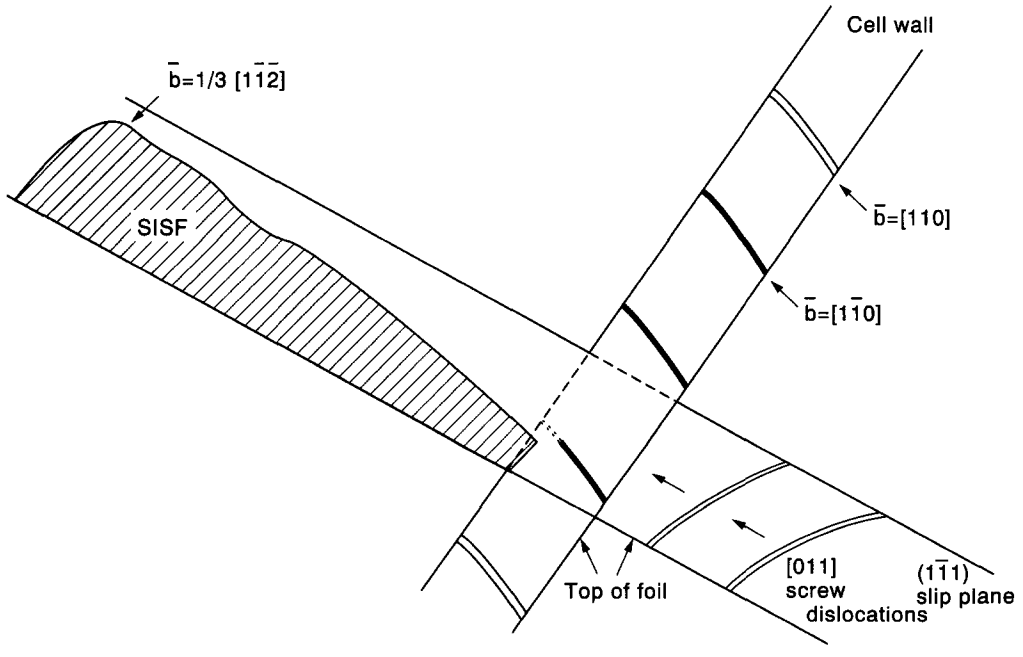

Fig. 7. Schematic view of the gliding dislocations, the low angle grain boundary (cell wall) and the SISF that is formed. The intersections of the slip plane of the gliding dislocations with the upper and lower surface of the thin foil are indicated. Also the intersection of the grain boundary plane and the foil surfaces has been indicated.

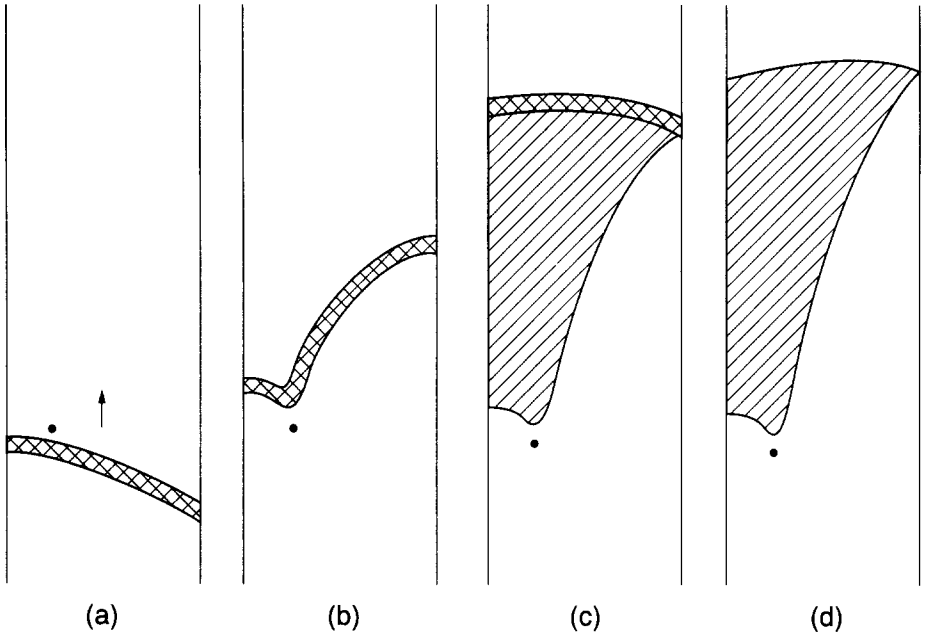

Fig. 8. Proposed SISF formation mechanism. Only the plane of the gliding dislocations is considered. The dislocation of the cell wall intersects the glide plane in a point, which is indicated. It is envisaged that the dislocation in the cell wall is actually dissociated into two superpartial dislocations very close to each other. Therefore the point actually represents two points very close to each other. (a) Dislocations gliding towards the intersection with the cell wall. The dislocations are each dissociated into two $\frac{1}{2}[011]$ superpartial dislocations connected by a ribbon of anti phase boundary (APB; double hatched). (b) After intersection, the gliding dislocation has a two jogs in its line and because of the pinning by the jogs it bows out under influence of the applied stress. (c) By the exchange of a $\frac{1}{6}[21\bar{1}]$ Shockley partial dislocation between the trailing $\frac{1}{2}[011]$ superpartial dislocation and the leading $\frac{1}{2}[011]$ superpartial, the region of APB (double hatched) between the partials is transformed into SISF (single hatched). (d) Because of the lower energy of the SISF the leading partial is allowed to move further in the glide direction.

to be elongated dislocation loops that were truncated because of the thinning process during preparation of the foil. Some observations were made of rows of loops of SISF of several hundred nm long. Pak *et al.* [20] made observations in Ni_3Ga, which is a very similar material to Ni_3Al, of widely extended SISFs with lengths of several hundreds of nanometers to a few μm, elongated along $\langle 110 \rangle$ directions and bounded by $\frac{1}{3}\langle 112 \rangle$ type partial dislocations. Veyssière *et al.* [22] made observations of two $\frac{1}{2}\langle 110 \rangle$ superpartials that were dissociated in a $\{100\}$ plane, connected by a ribbon of APB. Parts of one of the $\frac{1}{2}\langle 110 \rangle$ dislocations had dissociated in an inclined $\{111\}$ plane into a $\frac{1}{6}\langle 112 \rangle$ type edge Shockley partial and a $\frac{1}{3}\langle 112 \rangle$ type partial dislocation. These two dislocations were connected by a ribbon of SISF on the $\{111\}$ plane.

Several explanations have been put forward for the SISF formation. Pak *et al.* [20] explained the formation of loops bounding SISF's by means of an expanding perfect dislocation loop, which partially dissociates into two $\frac{1}{3}\langle 112 \rangle$ partial dislocations. Upon further expansion of the perfect loop, the SISF is elongated and finally, part of the SISF is pinched off and a faulted loop containing the SISF is created. Kear *et al.* [23, 24] discussed mechanisms by which gliding dislocations on intersecting slip planes could react and they showed that an SISF is formed in certain reactions. The mechanism described by Kear *et al.* is essentially a dislocation interaction mechanism involving two different slip planes, while the mechanism described by Pak *et al.* is essentially a single slip plane mechanism. Pak *et al.* do not go further into the reason of the initial dissociation of part of the perfect dislocation loop into $\frac{1}{3}\langle 112 \rangle$ partial dislocations. The SISF formation in our observations resembles the Pak *et al.* mechanism, as only one slip plane is involved. The creation of jogs in the line of the gliding dislocations because of the intersection with the dislocations in the cell wall could be the reason for the dissociation into $\frac{1}{3}\langle 112 \rangle$ partials under influence of the applied stress.

Comparison between modelling results and experimental observations

Our experimental observations of the interaction with the $\Sigma = 3$ coherent twin boundary can be compared to the computer modelling results, see also [4, 5]. The dislocation–grain boundary system that was studied is exactly the same as the system that is studied here experimentally and therefore, a one-to-one comparison is possible. The interaction mechanism that is observed in Ni_3Al in the simulations is the same as that which is observed in the *in situ* defor-

mation experiment. The magnitude of the stress at which transmission occurs cannot be compared so easily, as there is no experimental observation of a pile-up of dislocations against the grain boundary. From the number of dislocations in a pile-up and their spacing, the effective stress on the first dislocation near the boundary plane could be calculated. The friction stresses that are observed in the simulations are high in comparison with experiment and therefore the stresses that are necessary for transmission can be expected to be high as well.

The question may arise whether the observed behaviour is specific to Ni_3Al or exhibits a general feature of f.c.c. materials or of other $L1_2$ structured materials like Cu_3Au.

Observations of the same dislocation–grain boundary system were made in type 304 steel [25] and in 310 stainless steel [26]. Both materials have the f.c.c. structure. In 304 type stainless steel, a configuration in slightly deformed materials was observed which showed a pile-up of dislocations one side of the boundary and dislocations which appeared to have emerged on the other side. It was concluded that transmission through the twin boundary had taken place, equal to the results reported in this paper. The same mechanism of transmission of the same type of dislocations through the same boundary was observed in 310 steel during *in situ* deformation experiments [26].

However, in Cu_3Au absorption in the boundary plane was observed [5, 27], although there were a number of observations of transmissions as well. A possible explanation for the tendency to absorption could be found in a lower value of the energy of the ordering fault in the grain boundary plane between two $\frac{1}{2}[110]$ superpartial dislocations compared with the value of the APB between the superpartials in the bulk: i.e. in the order of 20 mJ/m^2 [4]. Thus regarding this energy difference absorption in the boundary might be expected, which of course is in contrast to f.c.c. materials since an ordering fault is not present, neither in the bulk nor grain boundary.

The main feature of Ni_3Al as compared with f.c.c. and other $L1_2$ materials like Cu_3Au lies in the stress level at which transmission through the boundary occurs [4]. The two superpartial dislocations in $L1_2$ constituting the arriving dislocation will decrease their separation in response to the applied stress, when the leading superpartial dislocation is halted at the boundary. In this way stress concentrations near the boundary will be generated which will increase upon increasing ordering tendency. Since the ordering tendency in Ni_3Al is much larger than in Cu_3Au the boundary in Ni_3Al will act as a much stronger obstacle for dislocation transmission.

CONCLUSIONS

Samples of Ni_3Al have been strained *in situ* in a TEM. The results of the *in situ* straining indicate that $\langle 110 \rangle$ screw dislocations impinging on a $\Sigma = 3$ coherent twin boundary that have a Burgers vector that is parallel to the grain boundary plane can be transmitted to the symmetric slip plane in the other grain under influence of an applied stress. A one-to-one comparison with the results of a computer modelling study of exactly the same system in Ni_3Al can be made and the experiment agrees with the simulations. Also, observations were made of superlattice intrinsic stacking faults (SISF) that were formed as a result of the interaction between gliding dislocations and the dislocations of a low angle grain boundary (cell wall). The creation of jogs in the line of the gliding dislocation may be the cause of the SISF formation.

Acknowledgements—This research is part of the research program of the Foundation for Fundamental Research on Matter (F.O.M.—Utrecht, The Netherlands) and has been made possible by financial support from The Netherlands Organization for Research (N.W.O.—The Hague, The Netherlands).

REFERENCES

1. K. Aoki and O. Izumi, *Nippon kink. Gakk.* **43,** 1190 (1979).
2. I. Baker, E. M. Schulson and J. A. Horton, *Acta metall.* **35,** 1533 (1987).
3. S. Hanada, T. Ogura, S. Watanabe, O. Izumi and T. Masumoto, *Acta metall.* **34,** 13 (1986).
4. B. J. Pestman, J. Th. M. De Hosson, V. Vitek and F. W. Schapink, *Phil. Mag. A* **64,** 951 (1991).
5. B. J. Pestman, J. Th. M. De Hosson, V. Vitek, F. D. Tichelaar and F. D. Schapink, *Alloy Phase Stability and Design* (edited by G. M. Stocks, D. P. Pope and A. F. Giamei), pp. 186, 253. MRS (1991).
6. J. J. Hauser and B. Chalmers, *Acta metall.* **9,** 802 (1961).
7. W. D. Brentnall and W. Rostoker, *Acta metall.* **13,** 187 (1965).
8. D. J. Dingley and R. C. Pond, *Acta metall.* **27,** 667 (1979).
9. M. Elkajbaji and J. Thibault-Desseaux, *Phil. Mag. A* **58,** 325 (1988).
10. L. P. Kubin and P. Veyssière, *Proc. 10th Int. Cong. Electron Microscopy*, Hamburg, W. Germany, p. 531. Deutsche Gesellscahft für Elektronenmikroskopie e.V. (Battelle-Institut e.V.) Frankfurt/Main (1982).
11. V. Vitek, G. J. Ackland and J. Cserti, *Alloy Phase Stability and Design* (edited by G. M. Stocks, D. P. Pope and A. F. Giamei), pp. 186, 237. MRS (1991).
12. A. P. Sutton and V. Vitek, *Phil. Trans. R. Soc. A* **309,** 37 (1983).
13. D. Farkas and E. J. Savino, *Scripta metall.* **22,** 557 (1988).
14. M. Yamaguchi, V. Paidar, D. P. Pope and V. Vitek, *Phil. Mag. A* **45,** 867 (1982).
15. Z. S. Basinski, M. S. Duesbery and R. Taylor, *Phil. Mag.* **21,** 1201 (1970).
16. P. B. Hirsch, A. Howie, R. B. Nicholson, D. W. Pashley and M. J. Whelan, *Electron Microscopy of Thin Crystals*, p. 156. Butterworths, London (1965).
17. J. M. Silcock and W. J. Tunstall, *Phil. Mag.* **10,** 361 (1964).
18. V. Vitek, R. C. Perrin and D. K. Bowen, *Phil. Mag.* **21,** 1049 (1970).

19. G. M. Bond, I. M Robertson and H. K. Birnbaum, *J. Mater. Res.* **2,** 436 (1987).
20. H. R. Pak, T. Saburi and S. Nenno, *Scripta metall.* **10,** 1081 (1976).
21. I. Baker and E. M. Schulson, *Physica status solidi* (a) **85,** 481 (1984).
22. P. Veyssière, J. Douin and P. Beauchamp, *Phil. Mag. A* **51,** 469 (1985).
23. B. H. Kear, A. F. Giamei and J. M. Oblak, *Scripta metall.* **4,** 567 (1970).
24. B. H. Kear, J. M. Oblak and A. F. Giamei, *Metall. Trans.* **1,** 2477 (1970).
25. W. A. T. Clark, R. H. Wagoner, *Dislocations in Solids* (edited by H. Suzuki, T. Ninomiya, K. Sumino and S. Takeuchi), p. 647. Univ. of Tokyo Press (1985).
26. T. C. Lee, I. M. Robertson and H. L. Birnbaum, *Metall. Trans.* **21A,** 2437 (1990).
27. F. D. Tichelaar and F. W. Schapink, *Phil. Mag. A* **62,** 53 (1990).